atmosphere

Article

Comparison of Air Pollutants during the Two COVID-19 Lockdown Periods in Winter 2019 and Spring 2022 in Shanghai, China

Yingxuan Li, Yanrong Yang * and Leying Zhang

Co-Innovation Center for Sustainable Forest in Southern China, College of Ecology and the Environment, Nanjing Forestry University, Nanjing 210037, China; lyx1020906908@163.com (Y.L.)
* Correspondence: yangyanrong@njfu.edu.cn

Abstract: During the winter of 2019, the global outbreak of COVID-19 prompted extensive research on urban air pollution under lockdown measures. However, these studies predominantly focused on winter conditions, thereby limiting investigations into changes in urban air pollutants during other seasons that were also subject to lockdown restrictions. Shanghai, China, has undergone two COVID-19 lockdown periods in two seasons: winter 2019 and spring 2022. The seasonal variations and human activities were represented by meteorological factors and nighttime light brightness in this paper, respectively. The reduction in human-related emissions during the two lockdown periods was estimated based on the targets outlined in China's Air Pollution Prevention and Control Action Plan. The results showed significant reductions in NO_2 and PM particles during the two lockdown periods, both accompanied by a notable increase in O_3 concentration. In comparison to the winter lockdown, there was an approximate 40% decrease in the NO_2 and $PM_{2.5}$ concentrations in the spring, while the O_3 concentration exhibited an increase of 48.81%. Furthermore, due to shifting wind patterns during the two lockdowns from winter to spring, the high-pollution core areas shifted 20–25 km southeastward in the spring. The PM particles and NO_2 concentrations exhibited a considerable impact from human activities, whereas the O_3 concentration was affected mostly by seasonal change and interactions among air pollutants. Compared to the corresponding non-lockdown condition, the concentration of CO decreased during the winter lockdown; however, it increased during the spring lockdown. The different change in CO concentration during the two lockdown periods was found to have a lower effect on the O_3 concentration than that caused by changes in meteorological factors and nitrogen oxide (NO, NO_2) concentrations. In summary, the impact of COVID-19 lockdown periods on urban air pollutants was more pronounced in spring compared to winter, and the interactions among air pollutants also underwent alterations.

Keywords: COVID-19 lockdown; air pollutants; Shanghai, China; seasonal change; human activities

check for updates

Citation: Li, Y.; Yang, Y.; Zhang, L. Comparison of Air Pollutants during the Two COVID-19 Lockdown Periods in Winter 2019 and Spring 2022 in Shanghai, China. *Atmosphere* **2024**, *15*, 443. https://doi.org/10.3390/atmos15040443

Academic Editor: Klaus Schäfer

Received: 27 February 2024
Revised: 29 March 2024
Accepted: 1 April 2024
Published: 3 April 2024

1. Introduction

The problem of air pollution occurred after the industrial revolution [1]. Currently, over 80% of the global population is exposed to polluted air [2], with $PM_{2.5}$ concentrations even exceeding the minimum safe value of 10 $\mu g \cdot m^{-3}$ stated by the World Health Organization. In China, the complex topography, diverse climate zones, and unbalanced economic development exacerbate the complexity of air pollution control [3,4], which has become a huge challenge in urban areas since the 21st century. According to the data reported by the Ministry of Ecology and Environment of China, 85–90% of the air pollutants in China are particulate matter (PM_x) particles. Currently, the six primary air pollutants routinely monitored in China are $PM_{2.5}$, PM_{10}, O_3, SO_2, NO_2, and CO [5].

The concentrations of air pollutants in China have gradually decreased since the implementation of China's Air Pollution Prevention and Control Action Plan in September

2013 [4,6]. The concentrations of pollutants rapidly decreased by 30–60% in the early part of 2020 due to the lockdown during the Corona Virus Disease 2019 (COVID-19) pandemic. COVID-19 broke out in Wuhan, China, and quickly swept across the world, and the ensuing worldwide lockdown promoted a remarkable reduction in human-related emissions and improved the air quality [7,8], especially in urban areas. The COVID-19 lockdown provided an important opportunity for studying urban air pollution.

The worldwide decreasing trends in air pollutants during the COVID-19 lockdown in the winter of 2019 have been verified based on observation data and numerical models, and the values in various places were slightly different. During the lockdown, large declines in the concentrations of nitrogen oxide (NO and NO_2) and PM particles ($PM_{2.5}$ and PM_{10}) were observed [9], and the concentration of O_3 increased. Due to the reduction in the nitrogen oxide concentration, the titration effect of NO on O_3 weakened, so the O_3 concentration exceeded the standard and was greater than that of $PM_{2.5}$, and thus, O_3 became the main air pollutant during the COVID-19 lockdown [10]. Due to the reduction in vehicle usage during the lockdown, the concentrations of $PM_{2.5}$ and PM_{10} in Los Angeles, CA, USA, decreased by about 17% [11], which was much less than the decrease in Suzhou, China [10], showing that the air pollution caused by human activities was more serious in the latter. In addition, in China, the concentration of SO_2 in Suzhou increased by 1.5% during the lockdown, while it exhibited a significant decrease of about 20% in Beijing, similar to the changes in the NO_2 and $PM_{2.5}$ concentrations [12].

The lockdown mainly affected human activities, which can be represented by the nighttime light brightness. It was found that the lights dimmed in 82% of the populated areas in China during the winter COVID-19 lockdown, and the decrease in India reached 87% [13]. In Wuhan, China, the light brightness in the evening after the COVID-19 lockdown ended was still lower than that before the pandemic [14]. In China, the reduction in air pollution caused by the lockdown was consistent with the aim of China's Air Pollution Prevention and Control Action Plan, so the estimated air pollution reduction during the lockdown period could be achieved by meeting this plan. For example, the estimated concentrations of air pollutants in Beijing were greatly reduced during the period of COVID-19, which was consistent with the true values; however, it was also estimated that the O_3 concentration greatly decreased [12]. The estimated O_3 concentration was not accurate; that is, the actual increase in O_3 during the lockdown in Beijing was not directly associated with human activities.

Many studies have been conducted on urban air pollution during the COVID-19 lockdown in the winter of 2019, but it is well known that COVID-19 did not stop at the beginning of 2020. With the development of the epidemic, the COVID-19 lockdown still sporadically continued in some regions of the world and probably happened in different seasons in the same areas. However, the urban air pollution differences under seasonal lockdown have not been studied, and the comprehensive impact of meteorological conditions and the lockdown has never been considered. Two such seasonal lockdown periods occurred in Shanghai, one of the largest cities in China, in the winter of 2019 and the spring of 2022. This provides a rare opportunity to study the seasonal variation of urban air pollutants under lockdown conditions. Under identical lockdown conditions, the disparity in air pollution between winter and spring was attributed to meteorological factors [15] as well as interactions among air pollutants [10,16,17]. It showed that the average temperature during the spring lockdown period in 2022 reached 18.69 °C, which was 11.74 °C higher than that during the winter lockdown period in 2019, and the monthly precipitation was 72.00 mm higher during the spring lockdown period. Enhanced solar radiation and precipitation play a favorable role in dispersing and diluting air pollutants such as $PM_{2.5}$, whereas higher temperatures facilitate the accumulation of O_3 [18,19]. Simultaneously, Shanghai exhibits a typical monsoon climate, necessitating the analysis of spatial variations in air pollution due to wind speed and direction changes [20]. Considering the lockdown conditions, this paper focuses on comparing the alterations in air pollutants during two distinct seasons. The aim is to elucidate the quantitative values and mechanisms of changes in urban air pollutants that are associated with human activities and meteorological factors, as well as interactions among air pollutants. The research holds significant implications for the analysis and mitigation of urban air pollution.

2. Data and Methods

2.1. Study Area

Shanghai, located at the southeast end of the Yangtze River delta of China (30°40′ N–31°53′ N, 120°52′ E–122°12′ E) with an average altitude of 2.19 m, is one of the most active areas for economic development, which leads to the diverse sources of air pollution, such as urban construction, transportation, industrial production, and straw burning in agricultural production, being very complex. Moreover, the flat terrain of Shanghai is also in the transition zone of China's southern and northern climates, indicating the accumulation of pollutants that are not easy to spread. In recent years, researchers have found that the main pollutants in Shanghai's air are $PM_{2.5}$, PM_{10}, NO_2, and O_3, which are mainly particulate pollutants in autumn and winter, and O_3 pollution in spring and summer [21]. Moreover, the 30-day lockdown in the winter of 2019, the new COVID-19 lockdown lasted 64 days in Shanghai from 28 March to 31 May 2022. The lockdowns would change the air pollution patterns in Shanghai.

Figure 1 shows the overview of Shanghai, indicating the location of Shanghai in China (Figure 1a), neighboring provinces of Shanghai and their distributions of urban, rural, and industrial land, which are classified as land designated for human activities (Figure 1b), as well as Shanghai's distributions of urban, rural, and industrial land as well as atmospheric environment monitoring stations (Figure 1c), and the administrative districts and the distribution of COVID-19 infections (per km^2) in the spring of 2022 in Shanghai (Figure 1d). As can be seen from Figure 1, the 9 districts (shown as blue box areas in Figure 1d), i.e., the main urban area in Shanghai, are the main human activity areas, major COVID-19 infection areas, and also have dense atmospheric environment monitoring stations. This main urban area has often been the core area of air pollution in Shanghai [22]. For the neighboring provinces of Jiangsu, Anhui, and Zhejiang, they are indeed the areas that affect Shanghai's air pollution [23,24], which can also be seen from the distributions of land for human activities in these provinces (Figure 1b).

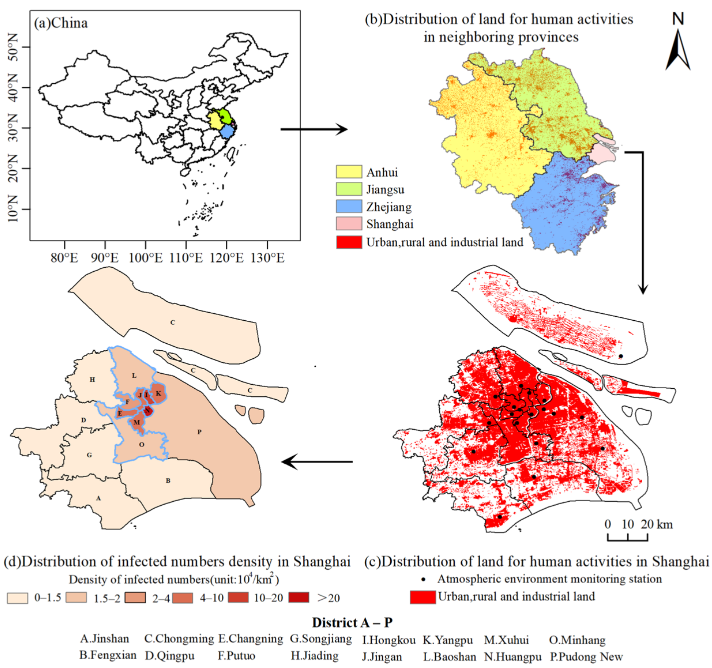

Figure 1. The overview map of Shanghai, China. There are four figures here. (**a**) is the administrative map of China, in which a small pink area means Shanghai, and its neighboring provinces are colored:

Jiangsu province in green, Anhui province in yellow, and Zhejiang province in blue. (**b**) shows an enlarged view of these three neighboring provinces and their distributions of urban, rural, and industrial land, that is, the land mainly for human activities (the land use data was from the Chinese Academy of Sciences: https://www.resdc.cn/data.aspx?DATAID=360, accessed on 10 December 2023). The areas for human activities in Zhejiang, Anhui, and Jiangsu account for 9.38%, 10.09%, and 19.06% of the total areas of the corresponding provinces, respectively. (**c**) shows Shanghai's distributions of urban, rural and industrial land and atmospheric environment monitoring stations. The symbol "·" in (**c**) represents the locations of the stations, totaling 19 in Shanghai. The area for human activities accounts for 43.02% of the whole of Shanghai. The overlap between the monitoring stations and areas of high human activity is evident in (**c**), as depicted in the blue box area in (**d**), encompassing 9 administrative regions including Baoshan, Jingan, Hongkou, Yangpu, Putuo, Changning, Huangpu, Xuhui, and Minhang, represented with letters L, J, I, K, F, E, N, M, and O, respectively, and the proportions of the land for human activities in each district are more than 43.02%. The letters A–P in (**d**) means the names of Shanghai's 16 administrative districts (see the legend on the bottom in Figure 1). (**d**) shows the map of Shanghai's administrative districts, with colors showing the distribution of COVID-19 infection density in spring 2022, i.e., the number of infections in one square kilometer the unit is $10^4/\text{km}^2$. The darker the color, the more people infected (the sum of the symptomatic and the asymptomatic); see the legend on the lower left. There were more than 60,000 confirmed cases and more than 540,000 asymptomatic infected people in this period.

2.2. Data

2.2.1. Data for the Air Quality Index and Six Air Pollutants

The hourly air quality index (AQI) values and the concentrations of six air pollutants were obtained from the website of the China National Environmental Monitoring Center (https://106.37.208.233:20035/, accessed on 12 December 2022). The ArcGIS software (version 10.8) was employed to process the daily data into monthly data with a spatial resolution of $0.1° \times 0.1°$ grids, and the spatiotemporal changes in the concentrations of the pollutants in winter and spring in Shanghai during the background and after and before lockdown periods were analyzed.

2.2.2. Nighttime Light Brightness

The nighttime light brightness data, which reflect human activities, were obtained from the National Polar-Orbiting Partnership-Visible Infrared Imaging Radiometer Suite (NPP-VIIRS) product provided by the National Aeronautics and Space Administration (NASA) (https://eogdata.mines.edu/download_dnb_composites.Html, accessed on 22 January 2023). Clipping was performed using the ArcGIS tool with the research area as a mask. The nighttime light brightness values in the various regions and time periods were obtained, and the changes in the brightness samples in Shanghai during the after and before lockdown periods were observed.

2.2.3. Seasonal Meteorological Data

The historical meteorological data for Shanghai were from Songjiang Station in Shanghai (https://data.cma.cn/, accessed on 22 November 2022), with an hourly temporal resolution. To analyze the influence of the seasonal meteorological differences in winter and spring on the concentrations of air pollutants, we took the historical data for the same period during the winter and spring lockdown periods and calculated the daily mean values to represent the meteorological conditions, which include the air temperature, precipitation, wind speed, and wind directions. Here, wind direction and speed were represented by wind-roses diagrams to analyze the impact of monsoon changes on the spatial distribution of air pollutants under winter and spring lockdowns in Shanghai. The wind-rose diagrams showed 16 directions of wind, as well as the occurrence probabilities and wind speeds.

2.3. Methods

2.3.1. Estimation of Human-Related Emission Reduction of Air Pollution during Lockdown Periods

In China, the Air Pollution Prevention and Control Action Plan was implemented in 2013. Its aim is to reduce emissions of air pollutants associated with human activities, which are consistent with the results of the urban lockdown. Thus, the effect of human-related emission reduction during the lockdown periods was estimated using Equations (1) and (2) [12], taking the spring lockdown in 2022 as an example.

$$\rho_{2022AF\ estimation} = \frac{\rho_{2022BF}}{\rho_{2021BF}} \times \rho_{2021AF} \quad (1)$$

$$\rho_{2022AF\ AER} = \rho_{2021AF} - \rho_{2022AF\ estimation} \quad (2)$$

where $\frac{\rho_{2022BF}}{\rho_{2021BF}}$ in Equation (1) is the ratio of the air pollutant concentration during the *BF* period in 2022 (ρ_{2022BF}) to that during the same period in 2021 (ρ_{2021BF}). This ratio was seen as the anthropogenic emission reduction factor for 2022 compared with 2021. When multiplied by the concentration in 2021 at the same period as the *AF* in 2022, recording as ρ_{2021AF}, it can predict the air pollutant value during the *AF* period in 2022, i.e., $\rho_{2022AF\ estimation}$. In Equation (2), $\rho_{2022AF\ AER}$ is the anthropogenic emission reduction (*AER*) estimation during the *AF* period in 2022. The estimating method during the winter lockdown in 2019 is similar.

2.3.2. The Statistical Methods in Analysis

For the AQI and air pollutants' spatial distributions, we used kernel density analysis [23] to generate a continuous density surface from 16 discrete observation stations by interpolation, so as to express the spatial clustering or spatial distribution pattern of air pollutants and AQI in Shanghai.

For the time processing of AQI and air pollutants data, we used the statistical method of Mann–Kendall trend test, which is one of the more effective methods applied in trend detection analysis [24]. The test is a nonparametric statistical test that does not require the sample to obey a certain distribution, is not disturbed by a few outliers, has a high degree of quantification, and has a wide detection range.

The Pearson correlation coefficient is employed to quantify the relationship between AQI and air pollutants, with values ranging from −1 to 1. A correlation coefficient closer to 1 or −1 indicates a stronger association, while a value closer to 0 suggests a weaker connection. In this study, we analyze the Pearson correlation coefficients between AQI and air pollutants during winter and spring lockdown periods as a foundation for investigating their interaction changes.

We called the Python scikit-learn library to construct a linear regression model for computing the coefficient of determination R^2 [25] between the daily average meteorological factor values and the corresponding daily average air pollutant concentrations. A value closer to 1 indicates a stronger correlation, while proximity to 0 suggests a weaker correlation.

2.3.3. Specific Period Setting

We are already familiar with the COVID-19 lockdown in winter in China, and a new round of strict lockdown periods was from 28 March to 31 May 2022, in Shanghai. In this paper, based on changes in the air pollutants during the lockdown in the winter of 2019, the spring lockdown period in 2022 was taken as the main study period for comparing the seasonal changes in six air pollutants. For the purpose of comparison, both lockdown processes were implemented in three distinct time periods, i.e., the same historical period as the lockdown (the background period, i.e., the *BG*), the lockdown period (after lockdown period, i.e., the *AF*), and the previous month period before the lockdown (before lockdown, i.e., the *BF*). The *AF*, *BF*, and *BG* details in the winter and spring are shown in Table 1.

Table 1. The corresponding dates of *AF*, *BF*, and *BG* of the winter and spring lockdown periods.

Period	Winter Lockdown	Spring Lockdown
AF	From 26 January to 25 February 2020	From 28 March to 31 May 2022
BF	From 25 December 2019 to 25 January 2020	From 26 February to 27 March 2022
BG	From 26 January to 25 February for 2016–2019	From 28 March to 31 May for 2017–2021 except 2020

3. Results

3.1. Differences in Spatiotemporal Characteristics of Air Pollutants during COVID-19 Lockdown Periods in Winter and Spring

Figure 2 shows the air pollutant concentrations during the BG, BF, and AF periods in spring 2022 in Shanghai. Compared to the BG period, the AQI value decreased from 61.17 to 43.55, with a decline of 28.80%. Among the six primary air pollutants, the decline in the NO_2 concentration was the most significant, followed by the concentrations of PM_{10} and $PM_{2.5}$. The rates of decrease were as follows: NO_2 (58.14%) > PM_{10} (42.31%) > $PM_{2.5}$ (38.50%) > SO_2 (21.77%). The CO concentration increased. Compared to the BF period, the AQI value decreased by 17.25% during the AF period, and NO_2 still exhibited the largest decline. The rates of decrease were as follows: NO_2 (29.12%) > PM_{10} (23.66%) > $PM_{2.5}$ (10.54%). In addition to the concentration of CO, the SO_2 concentration also increased slightly. The O_3 concentration significantly increased during the AF period, and it was 16.60% and 33.76% higher than that during the BG and BF periods, respectively.

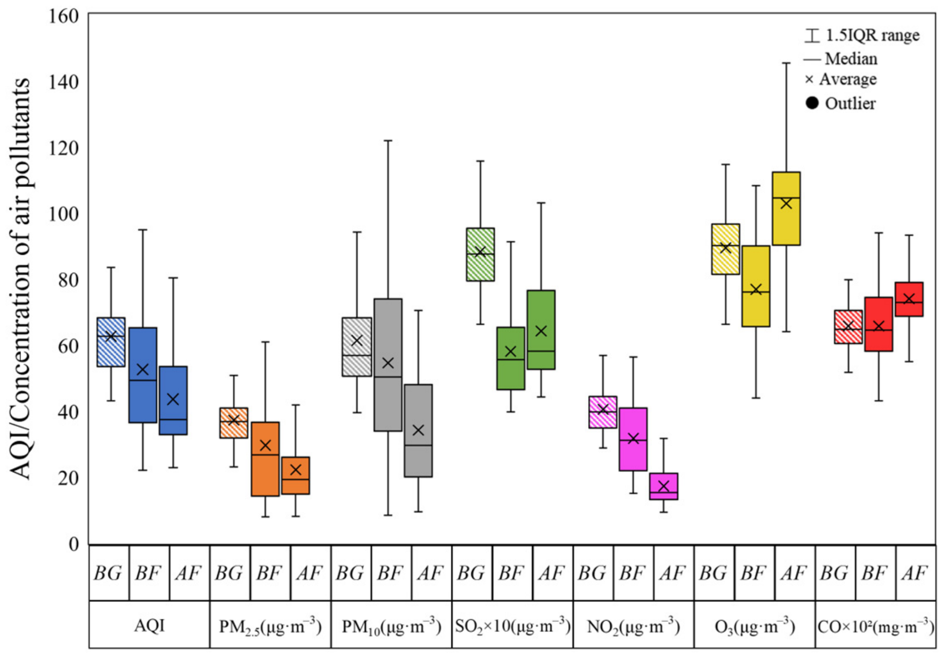

Figure 2. The AQI values and concentrations of air pollutants during the *BG*, *BF*, and *AF* periods in the spring of 2022. The AQI values and concentrations of $PM_{2.5}$, PM_{10}, SO_2, NO_2, O_3, and CO are represented by blue, orange, gray, green, pink, yellow, and red, respectively, and there are three values in each group. Take the AQI values as an example; the first one from the left represents the AQI value during the *BG* period, followed by those during the *BF* and *AF* periods. In the figure, "×" indicates the mean value, and "-" is the median value.

The details of the AQI and air pollutants during the winter and spring lockdowns are presented in Table 2. Based on the values in the first four rows of Table 2, the trends of the AQI, $PM_{2.5}$, PM_{10}, and NO_2 were completely consistent during the two AF periods, and they decreased compared to those during the corresponding BG and BF periods (the change rate columns in Table 2), with the rates of decrease being about 20–60%. During the two lockdown periods, the AQI, $PM_{2.5}$, PM_{10}, and NO_2 values (the AF period column in Table 2) in spring were all lower than those in winter, with rates of decrease of 19.84%, 40.92%, 7.00%, and 36.43%, respectively. This led to the fact that during the spring lockdown, the AQI value decreased to 43.55, i.e., an excellent grade of air quality according to the Chinese standard of grading per 50. In contrast, the changes in the O_3, SO_2, and CO concentrations were different (last three columns in Table 2). Compared to the corresponding BG and BF periods (change rate column in Table 2), both the spring and winter lockdowns resulted in increases in O_3. Additionally, the spring lockdown led to a slight increase in the CO concentration, with a lower rate of increase compared to that of O_3. However, during the winter lockdown, the CO concentration decreased. The change in the SO_2 concentration was complex. Compared to the BF and BG periods, the lockdown resulted in a general reduction in SO_2; however, this impact was weaker during spring. Compared to the BG period, the rates of decrease of the SO_2 concentration were 58.92% during the winter AF period and 21.77% during the spring AF period, with an unexpected increase of 10.53% during the spring lockdown compared to the spring BF period. During the two lockdown periods, the concentrations of O_3, SO_2, and CO increased in spring (the AF period column in Table 2), and O_3 exhibited the highest increase, which was 48.81% higher than that during winter.

Table 2. The AQI values and the concentrations of air pollutants during the two lockdown periods in Shanghai.

Variables	Winter	Spring	Winter	Spring	Winter	Spring	Difference *	Winter	Spring	Winter	Spring
								(*AF* vs. *BG*)		(*AF* vs. *BF*)	
AQI	73.88	61.17	72.61	52.63	54.33	43.55	−10.78	−26.47%	−28.79%	−25.18%	−17.24%
$PM_{2.5}$ ($\mu g \cdot m^{-3}$)	51.23	35.99	52.42	29.58	37.46	22.13	−15.33	−26.88%	−38.50%	−28.55%	−25.19%
PM_{10} ($\mu g \cdot m^{-3}$)	66.79	58.96	44.82	54.65	36.56	34.01	−2.55	−45.27%	−42.31%	−18.44%	−37.76%
NO_2 ($\mu g \cdot m^{-3}$)	39.55	39.27	49.94	31.67	27.09	17.22	−9.87	−31.52%	−56.14%	−45.76%	−45.61%
SO_2 ($\mu g \cdot m^{-3}$)	14.80	8.20	6.90	5.81	6.08	6.42	0.34	−58.92%	−21.77%	−11.89%	10.53%
CO ($mg \cdot m^{-3}$)	0.84	0.65	0.83	0.66	0.66	0.74	0.08	−21.42%	13.85%	−20.92%	12.12%
O_3 ($\mu g \cdot m^{-3}$)	53.34	88.11	43.14	76.81	69.04	102.74	33.7	29.44%	16.60%	60.05%	33.76%

Note: the difference * in Table 2 means the values during the *AF* period in spring minus those during the *AF* period in winter. All the AQI values and the concentrations of air pollutants refer to average values during the corresponding periods; the specific time period is shown in Table 1.

The spatial distributions of the AQI and air pollutant concentrations are depicted in Figure 3. By comparing the two AQI values during the AF period, it was found that the implementation of the lockdown in spring (1st row and 3rd column in Figure 3) led to a displacement of the high-valued core area from the main urban area (see the nine districts shown as blue boxes in Figure 1d) toward the southeastern part of the Pudong New District in Shanghai. The NO_2, $PM_{2.5}$, and PM_{10} concentrations also exhibited this displacement. Combined with Figure 1c, it was shown that the main urban area of Shanghai was the area with high levels of human activity; however, the two COVID-19 lockdowns both resulted in the most significant reductions in AQI and concentrations of $PM_{2.5}$, PM_{10}, and NO_2 observed in this area (Figure 3). Regarding the spring conditions (first three columns in Figure 3), there was a more pronounced decline in the AQI, NO_2, and SO_2 values in the western region of Shanghai (indicated approximately by the black dashed line in the AQI distribution figure during spring AF) compared to those observed during the BG and BF periods, and there was even a slight increase in the SO_2 concentration within the Pudong New District during the AF period compared to the BF period.

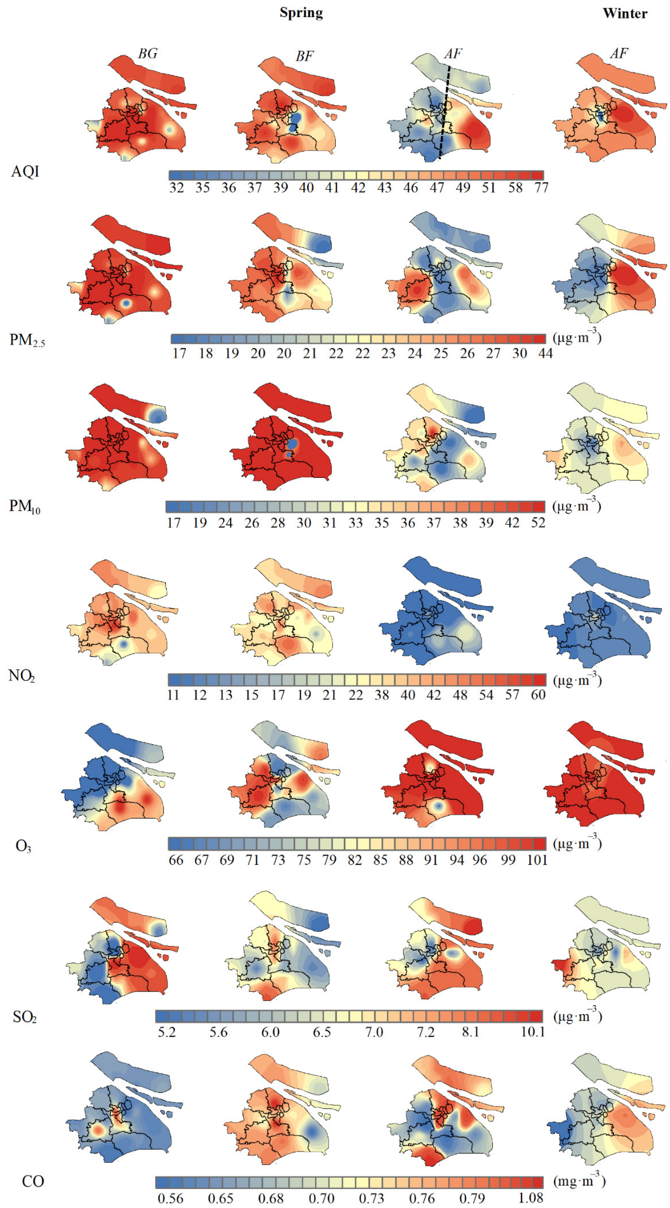

Figure 3. Spatial distribution of AQI values and concentrations of six primary pollutants in Shanghai. The first three columns, from left to right, mean: *BG* period, *BF* period, and *AF* period in spring 2022, respectively; the last one shows the distribution during the *AF* period in the winter of 2019. Each row from top to bottom means the distribution of AQI, $PM_{2.5}$, PM_{10}, SO_2, NO_2, O_3, and CO, respectively. The units for $PM_{2.5}$, PM_{10}, SO_2, NO_2, and O_3 are $\mu g \cdot m^{-3}$; CO is $mg \cdot m^{-3}$.

3.2. Quantitative Assessment of the Impact of Human Activities on Air Pollution during the COVID-19 Lockdown Period

3.2.1. Nighttime Light Brightness and Air Pollutants during the Two AF Periods

The distribution of the nighttime light brightness difference between the *AF* and *BF* periods during the two lockdown periods is shown in Figure 4. It can be seen that the decline in the maximum areas was concentrated in the main urban areas such as Changning, Xuhui, and Huangpu districts, with values of -3 $cm^{-2} \cdot sr^{-1} \cdot grid^{-1}$ and -5 $cm^{-2} \cdot sr^{-1} \cdot grid^{-1}$. In these areas, the decline area was smaller during the winter lockdown (Figure 4a) than during the spring lockdown (Figure 4b). The average urban nighttime light brightness decreased by about 2 $cm^{-2} \cdot sr^{-1} \cdot grid^{-1}$ during the two *AF* periods, indicating that a decrease in human activities occurred during the two lockdown periods.

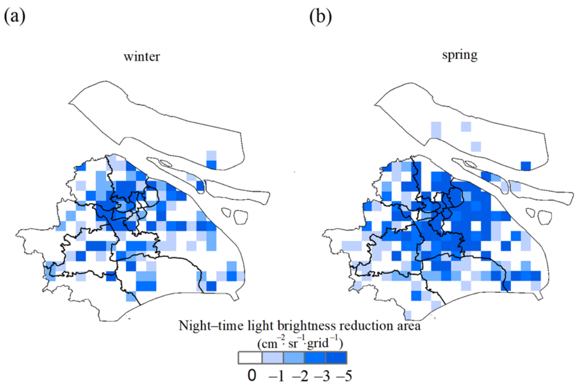

Figure 4. Nighttime light brightness differences between *AF* and *BF* periods during the two lockdown periods. (**a**,**b**) show the different distribution during the lockdown period in the winter of 2019 and the spring of 2022, respectively. Unit: $cm^{-2} \cdot sr^{-1} \cdot grid^{-1}$, the grid unit is $0.1° \times 0.1°$.

As mentioned above, the NO_2 and PM particle concentrations decreased the fastest during the two *AF* periods, which was closely related to the decrease in human-related emissions from mobile sources. The difference in the nighttime light brightness data between the *AF* and *BF* periods was compared with the difference in the NO_2 between the *AF* and *BF* periods, as well as the difference in the $PM_{2.5}$ concentration (Table 3). The results suggested that the decline in the nighttime light brightness was quite consistent with the decreases in the NO_2 and $PM_{2.5}$ concentrations. In both the winter and spring lockdown periods, the decline in nighttime light brightness exhibited a positive correlation with the decreases in the decline of NO_2 and $PM_{2.5}$ concentrations, with R^2 values of about 0.4 in 16 districts in Shanghai.

Table 3. The nighttime light brightness difference between *AF* and *BF* periods compared with the corresponding $PM_{2.5}$ (and NO_2) concentration differences in Shanghai.

Nighttime Light Brightness Difference ($cm^{-2} \cdot sr^{-1} \cdot grid^{-1}$)		**$PM_{2.5}$ ($\mu g \cdot m^{-3}$)**		**NO_2 ($\mu g \cdot m^{-3}$)**	
winter	spring	winter	spring	winter	spring
−1.56	−5.07	−13.65	−17.16	−21.68	−25.19
−4.53	−3.82	−17.23	−6.28	−22.11	−28.22
−2.42	−2.14	−18.76	−14.80	−25.67	−17.17
−6.77	−3.25	−17.80	−7.92	−22.71	−17.57
−8.49	−2.79	−18.63	−12.85	−22.60	−23.12
−4.02	−5.24	−18.53	−15.04	−23.35	−20.02
−4.57	−1.70	−16.03	−8.54	−25.51	−21.86
−2.56	−3.46	−15.20	−16.97	−12.10	−10.27
−4.23	−0.93	−11.50	−6.68	−30.20	−8.13
−2.63	−0.94	−10.10	−8.90	−24.30	−22.13
−0.65	−1.10	−14.60	−7.34	−19.96	−12.09
0.28	−0.08	−4.20	−3.68	−5.15	−4.26
−0.19	−0.62	−6.53	−6.96	−14.40	−14.82
−0.72	−0.53	−18.23	−7.16	−24.80	−15.19
−0.14	−0.99	−6.80	−7.65	−7.80	−8.65
−0.07	−0.15	−11.56	−11.64	−8.01	−6.09

3.2.2. Estimation of Human-Related Emission Reduction during the Two Lockdown Periods

The estimates of the human-related emission reduction during the *AF* periods in spring 2022 and winter 2019 in Shanghai are presented in Table 4. The local emission estimates exhibit a good correlation with the actual air pollutant concentrations, with fitting coefficients of 0.96 and 0.99 for spring and winter, respectively. The estimated reductions in human-related $PM_{2.5}$, PM_{10}, and NO_2 emissions during the two lockdown periods exhibit positive trends, indicating an immediate effect on the decreases in these three air pollutants due to reduced anthropogenic activities. However, an increase in the O_3 concentration was observed during both lockdown periods, suggesting that it was not solely produced by human activities or had little direct correlation with them. Consequently, a reduction in O_3 emissions related to human activities could not be achieved. Nevertheless, the specific impacts of the lockdowns on the above four air pollutants varied in the two different seasons. For instance, the estimated increase in the O_3 concentration was more significant during the spring lockdown than that during the winter lockdown, with the values of human-related emission reduction being –6.29 $\mu g \cdot m^{-3}$ and –17.71 $\mu g \cdot m^{-3}$ in winter and spring (Table 4), respectively, and the anthropogenic $PM_{2.5}$ emission reduction was also larger in the spring lockdown than that in the winter lockdown. This variation may be attributed to factors such as seasonal differences between winter and spring or mutual interactions among the air pollutants. For SO_2 and CO, the anthropogenic emission reduction exhibited a positive trend during the winter lockdown and a negative trend during the spring lockdown, and the difference change was more significant for SO_2 during the two lockdown periods than that of CO.

Table 4. Estimates of human-related emission reduction during the two lockdown periods in Shanghai.

		$PM_{2.5}$	PM_{10}	SO_2	NO_2	O_3	CO
Local emission estimates	winter	39.42	35.37	4.89	29.78	65.63	0.72
($\mu g \cdot m^{-3}$)	spring	25.50	51.10	7.62	23.71	97.63	0.72
Human-related emission reduction	winter	2.36	14.34	1.45	5.56	−6.29	0.02
($\mu g \cdot m^{-3}$) *	spring	5.72	6.72	−1.13	5.54	−17.71	−0.05
Rate of change **	winter	−23.10%	−45.84%	−49.99%	−37.76%	11.44%	−2.41%
	spring	−48.50%	−46.21%	9.60%	−38.54%	39.81%	9.97%

Note: * "Human-related emission reduction" comes from Equation (2). ** "Rate of change" refers to the variation between estimated values during the *AF* period and the observed values during the corresponding same period in the previous year. Except the unit of CO is $mg \cdot m^{-3}$, the rest of the air pollutants are $\mu g \cdot m^{-3}$.

In Table 4, under the same lockdown scenario, the estimation of the anthropogenic NO_2 emission reduction was highly consistent in winter and spring, with an average decrease of 5.55 $\mu g \cdot m^{-3}$ (about 38% compared to the corresponding period in the previous year). Similarly, the PM_{10} concentration exhibited a similar rate of decrease of about 45% during the winter and spring *AF* periods. These findings suggest that of all the six air pollutants, NO_2 and PM_{10} were primarily driven by human activities and minimally influenced by seasonal variations.

3.3. Impact of Seasonal Differences on Air Pollution during the Two COVID-19 Lockdown Periods

To investigate the impact of meteorological variations from winter to spring on the air pollutant changes in Shanghai, the scatter plot in Figure 5 depicts the correlation between the daily mean temperature and average daily levels of $PM_{2.5}$ (and O_3) in Shanghai during the non-lockdown winter and spring periods in 2021. It is evident that the $PM_{2.5}$ concentration decreased slightly with increasing temperature from winter to spring (R^2 = 0.23), while the O_3 concentration increased significantly with increasing temperature (R^2 = 0.71). Based on Figure 5, it was calculated that for every 1 °C increase in temperature, there was an associated decrease of 1.01 $\mu g \cdot m^{-3}$ in the $PM_{2.5}$ concentration and an increase of 2.80 $\mu g \cdot m^{-3}$ in the O_3 concentration.

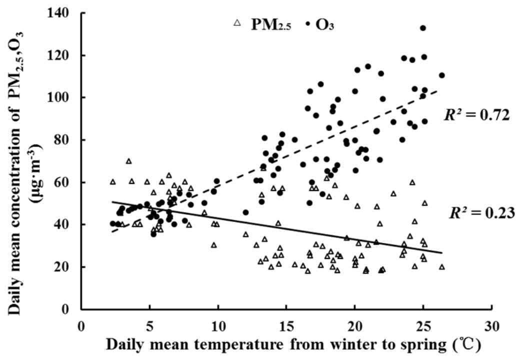

Figure 5. Daily mean temperature and $PM_{2.5}$ (O_3) scatter plots from winter to spring in Shanghai, covering the period from 26 January to 25 February (winter) and 28 March to 31 May 2021 (spring). A total of 96 fitting points were generated for the relationship between average daily temperature and $PM_{2.5}$ (O_3) concentration. The trend line of the relationship between temperature and O_3 is a dotted line, and that between temperature and $PM_{2.5}$ is a real line. Air temperature is measured in °C, while $PM_{2.5}$ and O_3 concentrations are measured in $\mu g \cdot m^{-3}$.

The spatial distribution of air pollution during the two lockdown periods in winter and spring was also influenced by meteorological factors. Compared to the non-lockdown conditions, during both *AF* periods, the air pollution cores shifted from the primary urban area (shown as blue box area in Figure 1d) toward the Pudong New District to the east (as depicted in Figure 3 for the change from *BF, BG* to *AF*), which was closely associated with Shanghai's typical monsoon climate, indicating the changes in wind patterns. The wind-rose diagram for the two lockdown periods is shown in Figure 6. It has been known that there was a relatively high concentration of inland air pollution in the adjacent provinces, such as Jiangsu and Anhui (Figure 1b) [23]. During winter and early spring (Figure 6a), air pollution occurred east of Shanghai (the *AF* period in winter, Figure 3), mostly due to northwestward airflow diffusion with wind speeds exceeding 4.5 m/s that brought the air pollutants from Jiangsu and Anhui and thereabout, combined with the flat terrain in Shanghai.

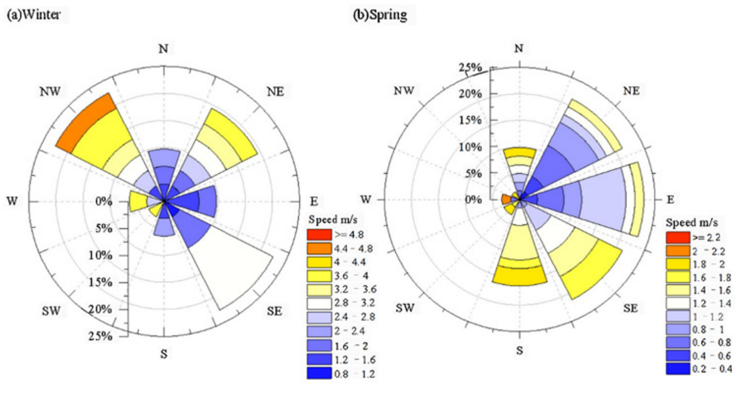

Figure 6. The wind-rose diagram for the two lockdown periods in winter 2019 (**a**) and spring 2022 (**b**).

However, compared to the locations of the core areas with high AQI, PM_{10}, and NO_2 values during the *AF* period in winter (Figure 3), the corresponding core areas shifted approximately 20–25 km southeastward during the *AF* period in spring, which was also attributed to changes in the wind direction caused by the monsoons (Figure 6b). The southward winds appeared in spring, with low wind speeds of 1–2 m/s, and transported pollutants originating in the neighboring province of Zhejiang (Figure 1b) toward the southern regions of Shanghai, resulting in their accumulation in the southern part of the city [24], while Zhejiang remained in non-lockdown conditions at this time. The southward shift in the air pollution core in spring may be related to the easterly wind from the sea.

Shanghai is a coastal city in the eastern part of China. The eastern regions in Figure 6b exhibited a relatively weak eastward wind component (mostly less than 1 m/s), which was also due to the monsoon climate. Studies have shown that the proportion of Shanghai's air pollution caused by the plumes of ships is significantly greater in spring than that in winter [20], indicating that the contribution of ships to the total $PM_{2.5}$ concentration within tens of kilometers of Shanghai's coastal area reached 20–30% (2–7 $\mu g \cdot m^{-3}$) in spring, and this was also the core area of the AQI during the spring lockdown in 2022.

In summary, the weak eastward component may have transported air pollutants from the sea, which then accumulated in the eastern part of Shanghai. Together with the air pollution from Zhejiang Province transported by the south wind component, this caused the southeast shift of the core area of air pollution during the spring lockdown period compared with the condition in the period of winter lockdown.

3.4. Interplay of Air Pollutants during the Two COVID-19 Lockdown Periods

The Pearson correlation coefficients of the AQI and six primary pollutants are presented in Table 5. It indicated that there were no obvious disparities in the two seasons. The AQI exhibited a strong correlation with each pollutant ($p < 0.01$). The highest correlations were between the AQI and the PM particles ($PM_{2.5}$, PM_{10}) concentrations during both seasons ($r > 0.8$, $p < 0.01$), while the weakest correlations were between the AQI and the O_3 concentration. The $PM_{2.5}$ concentration exhibited high positive correlations ($p < 0.01$) with all of the air pollutants, except O_3.

Table 5. Pearson correlation coefficients among air pollutants and AQI during the two lockdown periods in Shanghai.

	Season	**AQI**	**$PM_{2.5}$**	**PM_{10}**	**SO_2**	**NO_2**	**O_3**	**CO**
AQI	Winter	1						
	Spring	1						
$PM_{2.5}$	Winter	0.98 **	1					
	Spring	0.82 **	1					
PM_{10}	Winter	0.84 **	0.78 **	1				
	Spring	0.89 **	0.55 **	1				
SO_2	Winter	0.46 **	0.49 **	0.41 **	1			
	Spring	0.34 **	0.39 **	0.31 **	1			
NO_2	Winter	0.52 **	0.56 **	0.47 **	0.59 **	1		
	Spring	0.43 **	0.57 **	0.31 **	0.39 **	1		
O_3	Winter	0.26 **	−0.27 *	0.31 **	−0.02 *	−0.36 **	1	
	Spring	0.15 **	−0.03 *	0.17 **	0.28 **	−0.26 **	1	
CO	Winter	0.74 **	0.78 **	0.65 **	0.44 **	0.55 **	−0.52 **	1
	Spring	0.45 **	0.66 **	0.27 **	0.27 **	0.51 **	−0.13 **	1

Note:"**" and "*" mean results at levels 0.01 and 0.05 (two-tailed), respectively. All correlation coefficients in Table 5 were calculated from the daily mean values of AQI and air pollutants.

During the two lockdown periods, there was a significant negative correlation between the O_3 concentrations and the NO_2 and CO ($p < 0.01$) concentrations (Table 2). Similar findings have been reported in other studies on COVID-19 lockdowns, such as those conducted in the Yangtze River Delta region of China [10] and Vienna, Austria [16]. It should be noticed that NO and NO_2 play crucial roles in both the production and consumption of O_3 within the atmospheric boundary layer. Equation (3) expresses the dissociation reaction of O_3.

$$NO + O_3 \rightarrow NO_2 + O_2 \tag{3}$$

It is also called the titration reaction of O_3 [26]. This led to an increase in O_3 due to the significant decreases in nitrogen oxides concentrations (NO and NO_2) during both *AF* periods.

The relationship between CO and O_3 is relatively complex. CO and nitrogen oxides are common precursors of O_3, and the chain reaction during the process of O_3 generation in the troposphere is as follows [17]:

$$CO + OH \rightarrow CO_2 + H \quad (4)$$

$$H + NO_2 + M \rightarrow HO_2 + M \quad (5)$$

$$HO_2 + NO \rightarrow NO_2 + OH \quad (6)$$

$$NO_2 + hv \rightarrow NO + O \quad (7)$$

$$O + O_2 + M \rightarrow O_3 + M \quad (8)$$

It should be noted that the reaction (6) competes with the reaction in Equation (9) and thus prevents the loss of ozone [17].

$$HO_2 + O_3 \rightarrow OH + 2O_2 \quad (9)$$

Comparing Equations (6), (7), and (9), it can be seen clearly that the contribution of CO as an ozone precursor depends on the concentration of nitrogen oxides (NO, NO_2). During the COVID-19 lockdown period, the nitrogen oxides exhibited the most significant reductions, thereby rendering Equation (9) dominant. Consequently, the reaction between CO and hydroxide radicals (OH) (Equation (4)) during the lockdown periods would decrease the O_3 concentration in the troposphere. As the concentration of CO decreased during the lockdown period, the O_3 concentration would increase. This process occurred during the winter lockdown in Shanghai (the CO concentration decreased, during the winter lockdown as shown in Table 2). However, under the same lockdown conditions in Shanghai, the concentration of CO in spring lockdown increased (Table 2). It is known that the CO concentration is primarily influenced by human activities [27], and this increase during the spring lockdown period can be attributed to the transmission of airflow from the surrounding areas that were not under lockdown. Consequently, it is expected that there should have been a reduction in the O_3 concentration during the spring lockdown period because of the increase in the CO concentration. However, this did not occur; the O_3 concentration increased more significantly during the spring lockdown than in the winter. This suggests that the impact of CO on O_3 may have been considerably less significant than both the seasonal warming effects experienced in spring and the reduction in the nitrogen oxide titration effect.

4. Discussions and Conclusions

4.1. Discussions

Compared to the countrywide COVID-19 lockdown in the winter of 2019, the spatial scope of the lockdown in the spring of 2022 was limited to Shanghai. However, with the transition from winter to spring, there was a significant change in weather conditions. This aspect is worth studying for comparison purposes. The findings across different seasons exhibit similarities that can be directly attributed to the lockdown itself. For instance, during the two COVID-19 lockdown periods in Shanghai, China, both showed a substantial decrease in NO_2, $PM_{2.5}$, and PM_{10} concentrations, while showing a significant increase in O_3 concentration [9,15,28,29]. These observations indicated that the lockdown had a pronounced inhibitory effect on the NO_2, $PM_{2.5}$, and PM_{10} concentrations which mostly originated from urban mobile sources. Table 5 revealed that the correlation coefficients between $PM_{2.5}$ and NO_2, SO_2 exhibit smaller magnitudes compared to those between $PM_{2.5}$ and PM_{10}, particularly regarding the correlation coefficients between $PM_{2.5}$ and SO_2, which fell below 0.5 during both seasons. This observation suggests that although these air pollutants primarily originate from anthropogenic activities, their sources are not identical or even diverse. Undoubtedly, the contribution of automobile exhaust to NO_2 and $PM_{2.5}$ is universally acknowledged, while SO_2 predominantly emanates from stationary sources such as factories and power plants [30]. Furthermore, intricate chemical relationships exist among air pollutants, which further complicates regional air pollution research. For the concentration of O_3, the reduced nitrogen oxide emissions contributed to increasing its levels through the titration effect [26,29,31]. In fact, a significant increase in O_3 concentrations occurred throughout China during the COVID-19 lockdown period in the winter of 2019.

In terms of the lockdown, it restricts human activities. The findings in this paper demonstrated that, regardless of winter or spring, the lockdown rapidly and significantly decreased concentrations of NO_2, $PM_{2.5}$, and PM_{10}. Therefore, understanding the impact of human activities on these pollutants was crucial. To simulate emission reductions resulting from human activities, we adopted an approach based on China's Air Pollution Prevention and Control Plan [32], whose results aligned with observations during lockdown periods [12], with R^2 values exceeding 0.95 for both lockdown periods in this paper. Some COVID-19-related studies often used concentration differences before and after lockdown to assess their influence on air pollutants [33,34]. Additionally, various machine learning algorithms were frequently used to estimate the human-related impact on air pollutants [35]. These investigations consistently conclude that nitrogen oxides and particulate matter are most affected by human activities—key factors influencing changes in AQI levels—all of these which are consistent with the conclusions in this paper. According to the harmonic model [36], it was found that COVID-19 lockdown measures had significantly reduced nitrogen oxide levels, while long term implementation of China's air pollution prevention and control plan primarily accounted for decreases in PM particles, SO_2, and CO levels.

However, distinct numerical differences in air pollutant concentrations were observed during different seasons under lockdown measures in Shanghai. The $PM_{2.5}$ and NO_2 concentrations were lower in the spring compared to that of in winter, while the O_3 concentration increased more in the spring. These findings align with a previous study that highlighted the influence of seasonal variations on air pollutants [37], especially for changes in temperature, wind, humidity, etc. The alteration of these meteorological factors will not only impact the concentration levels of air pollutants but also influence their spatial distribution patterns. For instance, this study revealed that during the lockdown period in Shanghai, there was a southeastward shift of approximately 20–25 km in the core of high pollution areas from winter to spring, which can be attributed to changes in wind patterns.

Specifically, the O_3 concentration during the spring lockdown significantly increased to 102.74 $\mu g \cdot m^{-3}$, surpassing both the value of 69.04 $\mu g \cdot m^{-3}$ recorded in Shanghai during the winter lockdown and the value of 85.30 $\mu g \cdot m^{-3}$ measured in Suzhou [10]. Interestingly, this contradicts the decreasing trend of the O_3 concentration observed in Taiwan and China [38]. Some researchers have suggested a potential link between the decreased PM particles' concentrations and the increased O_3 concentration [39]. Although our results support this notion based on Shanghai data, we did not find any explicit internal relationship between these variables within our study. We determined a strong correlation between the increase in O_3 and the rise in temperature from winter to spring, with each 1 °C increment resulting in a corresponding increase of 2.80$\mu g \cdot m^{-3}$ in the O_3 concentration. However, when compared to winter conditions, the warming-induced increase in O_3 was found to be only 32.09%, which was smaller than the increase of 48.81% during the lockdown periods from winter to spring. Hence, while rising temperatures play a significant role in augmenting O_3 concentration, it is necessary to consider other factors such as lockdown measures and interactions among air pollutants that may vary across seasons. For instance, it was observed that there was a decrease in the CO concentration during the winter lockdown in Shanghai, but an increase occurred during the spring lockdown period. As one of the precursors for O_3, the impact of CO on O_3 depends on nitrogen oxide concentrations [17,40,41]. However, no matter how the CO concentrations changed during lockdown periods, the O_3 concentration increased, implying a relatively weak influence of CO on O_3 dynamics. The findings suggest that O_3 exhibited greater sensitivity to variations in geographical regions and meteorological conditions; it was also influenced by the presence of air pollutants themselves.

Since the implementation of the Air Pollution Prevention and Control Action Plan in September 2013, nationwide levels of SO_2, CO, NO_2, and $PM_{2.5}$ have witnessed a decrease. However, in VOC-sensitive areas, reducing NO and NO_2 levels or increasing VOC levels may exacerbate ozone pollution. Additionally, under hotter and drier meteorological conditions, ozone concentrations tend to increase [42]. Research indicates that China's average O_3 levels surpass the global average, with an increased frequency of high O_3 levels [43]. Notably, significant O_3 pollution is observed in the Yangtze River Delta region due to elevated emissions of ozone precursors. Recent studies have revealed that O_3 has surpassed $PM_{2.5}$ as the primary local air pollutant source in Shanghai [44], thus emphasizing the need for focusing on O_3 treatment as a novel approach towards addressing air pollution issues.

4.2. Conclusions

The air pollution variations in Shanghai during the winter and spring lockdowns exhibited similarities. No matter what season it was, the NO_2, $PM_{2.5}$, and PM_{10} concentrations were reduced significantly and immediately through lockdown measures. However, lockdown measures did not directly influence the O_3 concentration; rather, they indirectly affected the O_3 concentration by reducing titration effects and decreasing nitrogen oxide emissions. For the spatial distribution, the areas with high concentrations of air pollutants shifted eastward toward the Pudong New District in the two lockdown periods.

However, the air pollution variations during the winter and the spring lockdowns exhibited disparities. The change trend of the air pollutants was more pronounced during spring lockdown period: the $PM_{2.5}$ and NO_2 concentrations both decreased more significantly, while the O_3 concentration exhibited a more substantial increase. Additionally, the pollution center shifted slightly southeastward in spring from that in winter. These alterations were due to changes in rising temperatures, increasing precipitation, and shifts in wind patterns. Notably, these changes were not solely caused by individual factors of meteorological or lockdown measures, and they resulted from the comprehensive impact of these factors, including the mutual influence of the air pollutants themselves, which also varied seasonally. The different change in CO concentration during the two lockdown periods was found to have a lower effect on the O_3 concentration than that caused by changes in meteorological factors and nitrogen oxide (NO, NO_2) concentrations, while the effect of nitrogen oxide titration on O_3 was consistent across the two lockdown periods.

Author Contributions: Conceptualization, Y.Y.; methodology, Y.Y., Y.L. and L.Z.; formal analysis, Y.Y. and Y.L.; investigation, Y.Y. and Y.L.; resources, Y.Y. and Y.L.; writing—original draft preparation, Y.Y. and Y.L.; writing—review and editing, Y.Y. and L.Z.; visualization, Y.L. and Y.Y. All authors have read and agreed to the published version of the manuscript.

Funding: This research was funded by the National Natural Science Foundation of China (grant number 31971670).

Institutional Review Board Statement: Not applicable.

Informed Consent Statement: Not applicable.

Data Availability Statement: The original contributions presented in the study are included in the article; further inquiries can be directed to the corresponding author.

Acknowledgments: We thank reviewers for their insightful suggestions and comments.

Conflicts of Interest: The authors declare no conflicts of interest.

References

1. Feng, T.; Du, H.; Lin, Z.; Chen, X.; Chen, Z.; Tu, Q. Green recovery or pollution rebound? Evidence from air pollution of China in the post-COVID-19 era. *J. Environ. Manag.* **2022**, *324*, 116360. [CrossRef] [PubMed]
2. Loxham, M.; Nieuwenhuijsen, M.J. Health effects of particulate matter air pollution in underground railway systems—A critical review of the evidence. *Part. Fibre Toxicol.* **2019**, *16*, 116–360. [CrossRef]
3. Huang, H.; Ho, K.F.; Lee, S.C.; Tsang, P.K.; Ho, S.S.H.; Zou, C.W.; Zou, S.C.; Cao, J.J.; Xu, H.M. Characteristics of carbonaceous aerosol in $PM_{2.5}$: Pearl Delta River Region, China. *Atmos. Res.* **2012**, *104–105*, 227–236. [CrossRef]
4. Cai, S.; Wang, Y.; Zhao, B. The impact of the "Air pollution prevention and control action plan" on $PM_{2.5}$ concentrations in Jing-Jin-Ji region during 2012–2020. *Sci. Total Environ.* **2017**, *580*, 197–209. [CrossRef] [PubMed]
5. Jiang, L.; He, S.; Zhou, H. Spatio-temporal characteristics and convergence trends of $PM_{2.5}$ pollution: A case study of cities of air pollution transmission channel in Beijing-Tianjin-Hebei Region, China. *J. Clean. Prod.* **2020**, *256*, 120–631. [CrossRef]
6. Zhou, C.; Chen, J.; Wang, S. Examining the effects of socioeconomic development on fine particulate matter ($PM_{2.5}$) in China's cities using spatial regression and the geographical detector technique. *Sci. Total Environ.* **2018**, *619*, 436–445. [CrossRef]
7. Wilder-Smith, A.; Freedman, D.O. Isolation, quarantine, social distancing and community containment: Pivotal role for old-style public health measures in the novel coronavirus (COVID-19) outbreak. *J. Travel Med.* **2020**, *27*, 10–16. [CrossRef]
8. Hashim, B.M.; AI-Naseri, S.K.; AI-Maliki, A. Impact of COVID-19 lockdown on NO_2, O_3, $PM_{2.5}$ and PM_{10} concentrations and assessing air quality changes in Baghdad, Iraq. *Sci. Total Environ.* **2021**, *754*, 141978. [CrossRef] [PubMed]
9. Sicard, P.; De Marco, A.; Agathokleous, E. Amplified ozone pollution in cities during the COVID-19 lockdown. *Sci. Total Environ.* **2020**, *735*, 139–542. [CrossRef]
10. Wang, H.; Miao, Q.; Shen, L.; Yang, Q.; Wu, Y.; Wei, H.; Yin, Y.; Zhao, T.; Zhu, B.; Lu, W. Characterization of the aerosol chemical composition during the COVID-19 lockdown period in Suzhou in the Yangtze River Delta, China. *J. Environ. Sci.* **2021**, *102*, 110–122. [CrossRef]
11. Lipsitt, J.; Chan-Golston, A.M.; Liu, J.; Su, J.; Zhu, Y.; Jerrett, M. Spatial analysis of COVID-19 and traffic-related air pollution in Los Angeles. *Environ. Int.* **2021**, *153*, 106531. [CrossRef]
12. Zhao, X.; Shen, N.C.; Li, L.J.; Wu, G.F.; Tao, J.; Zhao, W.J. Analysis of the changes of air pollutants in Beijing, Tianjin and Hebei during the COVID-19 epidemic and the influencing factors. *Environ. Sci.* **2021**, *42*, 1205–1214. [CrossRef]
13. Ghosh, T.; Elvidge, C.D.; Hsu, F. The Dimming of Lights in India during the COVID-19 Pandemic. *Remote Sens.* **2020**, *12*, 3289. [CrossRef]
14. Shao, Z.; Tang, Y.; Huang, X.; Li, D. Monitoring Work Resumption of Wuhan in the COVID-19 Epidemic Using Daily Nighttime Light. *Photogramm. Eng. Remote Sens.* **2021**, *87*, 195–204. [CrossRef]
15. Dong, J.B.; Chen, X.L.; Cai, X.B. Analysis of the temporal and spatial variation of atmospheric quality from 2015 to 2019 based on China atmospheric environment monitoring station. *J. Geogr. Inf. Sci.* **2020**, *22*, 13. [CrossRef]
16. Bauer, R.; Speringer, M.; Frühwirt, P.; Seidl, R.; Trautinger, F. Assessing excess mortality in Vienna and Austria after the first year of the COVID-19 pandemic. *Vienna Yearb. Popul. Res.* **2022**, *20*, 8. [CrossRef]
17. Fishman, J.; Crutzen, P.J. The origin of ozone in the troposphere. *Nature* **1978**, *274*, 855–858. [CrossRef]
18. Filonchyk, M.; Peterson, M. Air Quality Changes in Shanghai, China, and the Surrounding Urban Agglomeration during the COVID-19 Lockdown. *J. Geovis. Spat. Anal.* **2020**, *4*, 22. [CrossRef]
19. Aimac, N.; Hladnik, M.; Zaletel-Kragelj, L. The impact of temperature on tropospheric ozone in the Nova Gorica region. *J. Public Health* **2011**, *50*, 121–130. [CrossRef]
20. Liu, Z.; Lu, X.; Feng, J.; Fan, Q.; Zhang, Y.; Yang, X. Influence of ship emissions on urban air quality: A comprehensive study using highly time-resolved online measurements and numerical simulation in Shanghai. *Environ. Sci. Technol.* **2017**, *51*, 202–211. [CrossRef]
21. Tong, S.; Kong, L.; Yang, K. Characteristics of air pollution episodes influenced by biomass burning pollution in Shanghai, China. *Atmos. Environ.* **2020**, *238*, 117756. [CrossRef]
22. Liu, Y.; Yang, X.; Li, M.; Tan, J. Concentration prediction and spatial origin analysis of criteria air pollutants in Shanghai. *Environ. Pollut.* **2023**, *12*, 121535. [CrossRef] [PubMed]
23. Li, L.; Chen, C.H.; Huang, C.; Streets, D.G.; Huang, H.Y.; Zhang, G.F.; Wang, Y.J.; Jang, C.J.; Wang, H.L.; Chen, Y.R.; et al. Air quality and emissions in the Yangtze River Delta, China. *Atmos. Meas. Tech.* **2011**, *11*, 1621–1639. [CrossRef]
24. Li, X.; Wu, C.; Meadows, M. Factors underlying spatiotemporal variations in atmospheric $PM_{2.5}$ concentrations in Zhejiang Province, China. *Remote Sens.* **2021**, *13*, 3011. [CrossRef]
25. Borhani, F.; Majid, S.; Amir, H.; Rashidi, Y.; Noorpoor, A.; Maddah, S. Optimization Models for Reducing the Air Pollutants Emission in the Production of Insulation Bituminous. *Environ. Energy Econ. Res.* **2023**, *7*, 1–14. [CrossRef]
26. Karl, T.; Lamprecht, C.; Graus, M. High urban NO_x triggers a substantial chemical downward flux of ozone. *Sci. Adv.* **2023**, *9*, 2365. [CrossRef] [PubMed]
27. Dhumad, S.Z.; Jasim, O.Z.; Hamed, N.H. The evaluation of carbon monoxide emissions using regression analysis and GIS techniques. *IOP Conf. Ser. Earth Environ. Sci.* **2023**, *1129*, 012041. [CrossRef]
28. Xian, T.; Li, Z.; Wei, J. Changes in Air Pollution Following the COVID-19 Epidemic in Northern China: The Role of Meteorology. *Front. Environ. Sci.* **2021**, *41*, 886. [CrossRef]

29. Lonati, G.; Riva, F. Regional Scale Impact of the COVID-19 Lockdown on Air Quality: Gaseous Pollutants in the Po Valley, Northern Italy. *Atmosphere* **2021**, *12*, 264. [CrossRef]
30. Khuzestani, R.P.; Taheri, A.; Yeganeh, B. Long-range transport of sulfur dioxide emissions from external sources to Tehran. *Urban Clim.* **2023**, *49*, 101445. [CrossRef]
31. Wang, H.; Huang, C.; Tao, W. Seasonality and reduced nitric oxide titration dominated ozone increase during COVID-19 lockdown in eastern China. *NPJ Clim. Atmos.* **2022**, *5*, 24. [CrossRef]
32. Ren, C.; Yu, C.; Cao, S. Development of urban air environmental control policies and measures. *Indoor Built Environ.* **2022**, *32*, 299–304. [CrossRef]
33. Avdoulou, M.; Golfinopoulos, A.; Kalavrouziotis, I. Monitoring Air Pollution in Greek Urban Areas during the Lockdowns, as a Response Measure of SARS-CoV-2 (COVID-19). *Water Air Soil Pollut.* **2023**, *234*, 13. [CrossRef] [PubMed]
34. Pushpawela, B.; Shelton, S.; Liyanage, G.; Jayasekara, S.; Rajapaksha, D.; Jayasundara, A.; Das Jayasuriya, L. Changes of Air Pollutants in Urban Cities during the COVID-19 Lockdown-Sri Lanka. *Aerosol Air Qual. Res.* **2023**, *23*, 220223. [CrossRef]
35. Kumar, K.; Pande, B.P. Air pollution prediction with machine learning: A case study of Indian cities. *Int. J. Environ. Sci. Technol.* **2023**, *20*, 5333–5348. [CrossRef] [PubMed]
36. Gao, C.; Zhang, F.; Fang, D.; Wang, Q.; Liu, M. Spatial characteristics of change trends of air pollutants in Chinese urban areas during 2016–2020: The impact of air pollution controls and the COVID-19 pandemic. *Atmos. Res.* **2023**, *283*, 36465231. [CrossRef] [PubMed]
37. Dong, J.; Liu, P.; Song, H.; Yang, D.; Yang, J.; Song, G.; Miao, C.; Zhang, J.; Zhang, L. Effects of anthropogenic precursor emissions and meteorological conditions on $PM_{2.5}$ concentrations over the "2+26" cities of Northern China. *Environ. Pollut.* **2022**, *315*, 120392. [CrossRef] [PubMed]
38. Wong, Y.J.; Yeganeh, A.; Chia, M.Y.; Shiu, H.Y.; Ooi, M.C.G.; Chang, J.H.W.; Shimizu, Y.; Ryosuke, H.; Try, S.; Elbeltagi, A. Quantification of COVID-19 impacts on NO_2 and O_3: Systematic model selection and hyperparameter optimization on AI-based meteorological-normalization methods. *Atmos. Environ.* **2023**, *301*, 119677. [CrossRef]
39. Yu, Y.J.; Meng, X.Y.; Wang, Z.; Zhou, W.; Yu, H.X. Driving Factors of the Significant Increase in Surface Ozone in the Bei-jing-Tianjin-Hebei Region, China, during 2013–2018. *J. Environ. Sci.* **2020**, *41*, 106–114. [CrossRef]
40. Choi, Y.; Wang, Y.; Zeng, T.; Cunnold, D.; Yang, E.; Martin, R.; Chance, K.; Thouret, V.; Edgerton, E. Spring-time transitions of NO_2, CO and O_3 over North America: Model evaluation and analysis. *J. Geophys. Res.* **2008**, *113*, 4. [CrossRef]
41. Mao, H.T.; Talbot, R. O_3 and CO in New England: Temporal variations and relationships. *J. Geophys. Res.* **2004**, *109*, 11. [CrossRef]
42. Vingarzan, R. A review of surface ozone background levels and trends. *Atmos. Environ.* **2004**, *38*, 21. [CrossRef]
43. Lu, X.; Hong, J.; Zhang, L.; Cooper, O.R.; Schultz, M.G.; Xu, X.; Wang, T.; Gao, M.; Zhao, Y.; Zhang, Y. Severe Surface Ozone Pollution in China: A Global Perspective. *Environ. Sci. Technol. Lett.* **2018**, *5*, 4–494. [CrossRef]
44. Li, W. Characteristics of Atmospheric Pollution in a Chinese Megacity: Insights from Three Different Functional Areas. *Sustainability* **2023**, *15*, 2429. [CrossRef]